ON THE CALCULATION OF LAMINAR SEPARATION BUBBLES IN TWO-DIMENSIONAL INCOMPRESSIBLE FLOW

by

J.L. van Ingen

AGARD CP-168, Symposium on Flow Separation; Gttingen
1975

ON THE CALCULATION OF LAMINAR SEPARATION BUBBLES IN TWO-DIMENSIONAL INCOMPRESSIBLE FLOW

J.L. van Ingen

Department of Aeronautical Engineering, Delft University of Technology, Kluyverweg 1, Delft, The Netherlands.

(Paper no 11 presented at the AGARD Fluid Dynamics Panal Symposium on Flow Separation, Göttingen, 27-30 May, 1975, to be published in AGARD CP 168)

SUMMARY.

The following topics are discussed in the paper.

- A new laminar boundary layer calculation method is presented which combines the simplicity of Thwaites' method for the prediction of the momentum loss thickness θ with the accuracy of Stratford's two-layer method for the prediction of the position of laminar separation.
- Calculated boundary layer characteristics for arbitrarily prescribed pressure distributions in general show a singular behaviour at separation. It is shown that a real separating flow tends to adjust itself in such a way that the resulting pressure distribution prevents a singular behaviour of the boundary layer to occur. It appears that $m = -\frac{\theta^2}{\nu}\frac{dU}{dx}$ shows a maximum value at separation.
- A simple calculation method for the laminar part of the separation bubble is presented. The pressure distribution is not prescribed but it is determined from the calculation such that the separation streamline assumes a prescribed shape.
- An earlier method for the prediction of transition in attached boundary layers, based on linear stability theory, is extended to the case of separated flows.
- Two methods are discussed which might be used to predict whether reattachment of the turbulent shear layer will occur, thus leading to a closed separation bubble.
- Finally some results will be discussed of windtunnel experiments on two different models. The first model is the FX 66-S-196-V1 Wortmann airfoil; the second model consists of a circular cylinder with a tapered tail.

NOTATION

a	constant in Eq. (2)
b	constant in Eq. (2)
B	constant in Eq. (16)
c	reference length, equal to chord for airfoil; equal to radius for cylinder
g	profile parameter for velocity profiles with reversed flow, Eq. (12)
H	δ^*/θ
ℓ	$\frac{\tau_o\theta}{\mu U} = \{\frac{\partial(u/U)}{\partial(y/\theta)}\}_0$
L	$2\ell + 2m(2+H)$
m	$-\frac{\theta^2}{\nu}\frac{dU}{dx} = \{\frac{\partial^2 u/U}{\partial(y/\theta)^2}\}_0$
p	static pressure
P	$\frac{\theta^2_{sep}}{\nu}\frac{\Delta U}{\Delta x}$
r	m/m_{sep}
R_c	$\frac{U_{ref}\, c}{\nu}$
R_θ	$\frac{U\,\theta}{\nu}$
u	velocity component in boundary layer parallel to wall
U	velocity component at edge of boundary layer
U_{ref}	reference speed
$\bar{U}$	U/U_{ref}
$-\alpha_i$	spatial amplification rate, Eq. (23)
β	Falkner-Skan pressure gradient parameter, Eq. (13)
γ	angle at which the separation streamline leaves the wall; Fig. 1
δ^*	$\int_0^\infty(1-\frac{u}{U})dy$ displacement thickness
θ	$\int_0^\infty \frac{u}{U}(1-\frac{u}{U})dy$ momentum loss thickness
φ	angular distance around circular cylinder, measured from leading edge
ψ	streamfunction
σ_a	amplification factor, Eq. (23)
ν	coefficient of kinematic viscosity
τ_o	wall shear stress
ω	disturbance frequency, Eq. (22)

Subcripts

Bℓ	Blasius value
r	reattachment
sep	separation
tr	transition
0	at surface

ΔU change in edge-velocity over length of separation bubble; Fig. 1

x distance along the wall

$\bar{x}$ $\frac{x}{c}$

Δx length of separation bubble, Fig. 1

y distance normal to wall

z $g * m_{sep}$

1. INTRODUCTION

Although quite a number of important references is available on the subject of the laminar separation bubble in two-dimensional incompressible flow (see for instance refs. 1 through 6) a fully satisfactory engineering method for the prediction of the characteristics of these bubbles does not yet exist. The present paper tries to fill some of the gaps in our knowledge; it appears that a complete prediction of the bubble is now within our reach. Some of the problems in this field are illustrated by the well known picture of the pressure distribution(*) in the separation region (Fig. 1). First we have to determine the separation point S; downstream of S we usually find experimentally a flattening of the pressure distribution. This part of the pressure distribution is not known a priori but it should follow from the calculation. Most of the existing calculation methods assume a constant wall pressure within the bubble but this is only a good approximation at low Reynoldsnumbers. The next problem is to predict the position of transition T in the separated shear layer. Downstream of T we may find a rather steep pressure recovery curve, leading to reattachment at R. Often R is assumed to lie on the dotted pressure distribution curve which would occur without the presence of the bubble. Sometimes reattachment does not occur; the bubble "bursts" and of course a calculation method should be able also to predict this bursting.
In the following chapters the different problems, mentioned above will be discussed in turn.

2. PREDICTION OF THE SEPARATION POINT USING ENGINEERING METHODS.

A well known engineering method for the calculation of the laminar boundary layer is that due to Thwaites (ref. 7). The accuracy of the method is quite good for the prediction of the momentum loss thickness θ; it is less accurate in the prediction of the separation position.
The idea behind this method is to use the von Kármàn momentum integral relation and the first compatibility condition of the boundary layer in the form:

$$\frac{d}{dx}\left(\frac{\theta^2}{\nu}\right) = \frac{2\ell+2m(2+H)}{U} = \frac{L}{U} \quad \text{and} \quad m = -\frac{\theta^2}{\nu}\frac{dU}{dx} = \left\{\frac{\partial^2 u/U}{\partial(y/\theta)^2}\right\}_o . \tag{1}$$

Thwaites assumed that ℓ and H and hence L are unique functions of m which allows us to calculate ℓ, m, H, L and θ as functions of x. The required functions $\ell(m)$, H(m) and L(m) were deduced by Thwaites from a number of exact solutions of the laminar boundary layer equations which were available to him at that time.
The momentum integral equation can be integrated easily between two points x_1 and x_2 if a linear relation

$$L = a + bm , \tag{2}$$

is assumed between L and m (Thwaites took a=0.45; b=6). The result is

$$\left(\frac{U^b\theta^2}{\nu}\right)_{x=x_2} - \left(\frac{U^b\theta^2}{\nu}\right)_{x=x_1} = a\int_{x_1}^{x_2} U^{b-1}\,dx \tag{3}$$

As soon as $\theta(x)$ is known, m(x), $\ell(x)$ and H(x) follow from the compatibility condition and the relations $\ell(m)$ and H(m). This allows us to find the separation point and an approximation to the boundary layer velocity profile. As was remarked already the predicted values of θ are sufficiently accurate for engineering use. For the favourable pressure gradient case (m<0) also the velocity profile is rather accurate. For adverse pressure gradients (m>0) the velocity profile is less accurate and hence the separation position is not predicted accurately enough for the present purpose. This is due to the fact that

(*) In the present paper we will by "pressure distribution" not only denote p(x) but also U(x).

Thwaites' method belongs to the class where a fixed relation exists between ℓ and m so that separation (ℓ=0) is found at a fixed value of m.

An improved method has been obtained in which $\ell(m)$, H(m) and hence L(m) are allowed to depend on an extra parameter. This parameter is taken as m_{sep}, the value of $m = -\frac{\theta^2}{\nu}\frac{dU}{dx}$ at separation.

To introduce this improved method we refer to figs. 2 through 4 where $\ell(m)$, H(m) and L(m) have been plotted in the same way as Thwaites did for some special accurate solutions of the boundary layer equations. The selected solutions have in common that for zero pressure gradient (m=0) they all reduce to the Blasius flat plate boundary layer. The separation values for H and L fall neatly on curves which coincide with the curves representing the separation points in Head's two-parameter method (ref. 8).

For the range of values of m_{sep} which is of practical interest (m_{sep}>.068) it follows that a good approximation for L_{sep} is:

$$L_{sep} = .14026+10\ m_{sep} \quad \text{and hence} \quad H_{sep} = 3 + \frac{.07103}{m_{sep}} . \tag{4}$$

It follows that ℓ, H and L can be very nearly made unique functions of $r=m/m_{sep}$ when properly scaled (see fig. 5). In what follows Hartree's similar solutions of the Falkner-Skan equation have been used to define these functions.

Introducing m_{sep} as an extra parameter, to be determined later, the new method may now be defined as follows. For favourable pressure gradients (m<0) use $\ell(m)$, H(m) and $\ell(m)$ as for the Hartree flows for which m_{sep}=.06815. For adverse pressure gradients (m>0) use the scaled functions

$$\ell = \ell(r)\ ;\ \frac{L-.44105}{L_{sep}-.44105} = L^*(r)\ ;\ \frac{H-2.5911}{H_{sep}-2.5911} = H^*(r) \tag{5}$$

as determined from the results for the Hartree flows. The momentum integral equation can then be integrated once a starting value for θ is available. As in Thwaites' method the integration can be performed in the form (3) when using the linear approximation (2). Of course b now depends on the parameter m_{sep}; with (4) it follows that for m_{sep}>.068:

$$b = 10 - \frac{.30079}{m_{sep}} \quad \text{or} \quad m_{sep} = \frac{.30079}{10-b} \tag{6}$$

For favourable pressure gradients we use b=5.16, corresponding to the straight line connecting the stagnation point and the Blasius point in fig. 4; for all values of b we have a=.44105. For each value of b (or m_{sep}) a Thwaites type method is obtained. For large values of b the method gives late separation, for small values of b early separation is obtained.

Of course some additional information is needed to determine b. When analysing experimental results b may be chosen such that the experimentally determined separation point is reproduced. In cases where the separation point is not known a priori we use Stratford's two-layer method (ref. 9) in the version of Curle and Skan (ref. 10) to provide the separation position. Lack of space does not permit to give a more detailed account of the present method; details will be given in a forthcoming report by the present author (ref. 11). A few results to illustrate the method may be found in figs. 6 through 8.

Fig. 6 gives some results for the potential flow pressure distribution around a circular cylinder where $\bar{U}=\sin \bar{x}$; a comparison has been made with the accurate numerical results due to Terrill (ref. 12). Fig. 7 gives some results for the measured pressure distribution on a Wortmann airfoil (see section 8).

The free-stream speed for this particular case was such that a closed laminar separation bubble occured. Using the surface oil film technique the separation point was found at a distance of 48% of the chord downstream of the leading-edge(*). It should be noted that the curve of $\bar{U}$ vs.$\bar{x}$ becomes rather flat downstream of the separation point leading to a point of inflexion shortly upstream of the separation point. This appears to be characteristic for all measured pressure distributions in the vicinity of separation.

It follows from fig. 7 that the present method does not predict separation for b>7.23; in fact the calculation tends to the flat plate boundary layer far downstream. For b<7.23 we do find separation while ℓ tends to zero with $\bar{x}$ like $\ell \leftrightarrows \sqrt{\bar{x}_{sep}-\bar{x}}$. This is the type of singularity discussed by Goldstein (ref. 13) which always seems to occur when boundary layer calculations are performed for arbitrarily prescribed pressure distributions. For b=7.23 separation is predicted at $\bar{x}$=47.2% with a finite value of $\frac{d\ell}{d\bar{x}}$ at separation. Apparently the real flow adjusts itself such that the Goldstein singularity can be prevented.

(*) note that x is measured along the surface; hence at the trailing edge we have x>100% c.

It should be remarked that the behaviour for b>7.23 is very similar to what Schubauer found when applying Pohlhausen's method to the measured pressure distribution for an elliptic cylinder with observed laminar separation. Later, Hartree (ref. 14) using an accurate numerical method could only find separation when slightly modifying the observed pressure distribution. It is still an open question whether indeed a small experimental error in Schubauer's experimental results is responsible for the failure to predict separation or that small errors inherent in the boundary layer approximation and the neglect of the longitudinal surface curvature are responsible for it.

It is instructive to invert the present calculation method to find out to what extent the pressure distribution should be modified to produce a noticeable shift in the separation position. The full curves in fig. 8 give the values of ℓ (for b=7.23) and the values of $\bar{U}$ and $\frac{d\bar{U}}{d\bar{x}}$ in the neighbourhood of the separation point for the same case as was shown in fig. 7. The dotted curve for ℓ represents an arbitrarily modified shear stress distribution for x>45% producing separation at 46%. The dotted curves for $\bar{U}$ and $\frac{d\bar{U}}{d\bar{x}}$ indicate the modifications which have to be made to the pressure distribution to produce the changed wall shear stress. These modifications are certainly within experimental error. Hence an important conclusion must be that the accuracy to be obtained in the prediction of laminar separation may depend more on the accuracy of the pressure distribution data than on the level of sophistication of the calculation method.

3. SOME OBSERVATIONS ON THE CHARACTERISTICS OF THE SEPARATING LAMINAR BOUNDARY LAYER.

Laminar boundary layer calculations for arbitrarily prescribed pressure distributions in general show a singular behaviour at separation, such that τ_o and ℓ tend to zero as the square root of the distance to separation (Goldstein, ref. 13). It was shown in section 2 that this singular behaviour is reproduced by the present method. It was also observed that for a measured pressure distribution the singularity may be prevented by a proper choice of b. Therefore it seems possible that the boundary layer equations may remain applicable through separation if only the proper pressure distribution is used. It should be remembered however that very small deviations from this pressure distribution will restore the singular behaviour. Therefore we must refrain from prescribing the pressure distribution in the separation region. But we should prescribe a regular behaviour of some other quantity like τ_o, ℓ or the displacement thickness. A recent example of such a method is given by Carter in ref. 15. It is of course very easy to invert the present method and prescribe a quantity other than the pressure. In fact fig. 8 gave a first example of this procedure where $\ell(x)$ was prescribed rather arbitrarily.

In order to be able to proceed in this direction we should first gather more information about the exact behaviour of the viscous flow near separation. Therefore it is useful to recall here an analytical solution of the Navier-Stokes equations which is valid in a small neighbourhood of the separation point where the inertial forces can be neglected. (See Legendre, ref. 16; Oswatitsch, ref. 17; Batchelor, ref. 18, page 226). It follows that the separation streamline leaves the wall at an angle γ (fig. 1) which is determined by:

$$\tan(\gamma) = -3 \left\{ \frac{\frac{d\tau_o}{dx}}{\frac{\partial p}{\partial x}} \right\}_{sep} \qquad (7)$$

The streamlines can easily be calculated once γ is known; they follow from:

$$y^2(x \tan(\gamma) - y) = \text{constant} \qquad (8)$$

where x is the distance downstream of separation. For points at which the u-component of the velocity is zero we find $\frac{y}{x} = \frac{2}{3}\tan(\gamma)$ and hence

$$\frac{y_{u=0}}{y_{\psi=0}} = \frac{2}{3} \qquad (9)$$

The pressure gradient vector is at an angle $\frac{1}{3}\gamma$ with the wall and hence for shallow bubbles where γ is small the pressure gradient normal to the wall is small so that the boundary layer equations might still give a reasonable result.

If we start from the boundary layer equations and assume small values of u and v we can also arrive at the results (7) and (9). Here it is assumed a priori that $\frac{\partial p}{\partial x}$ is independent of y. The result (9) also follows from the expression for the velocity profile in the form:

$$\frac{u}{U} = \ell \frac{y}{\theta} + \tfrac{1}{2} m \left(\frac{y}{\theta}\right)^2 \qquad (10)$$

which is valid for a sufficiently small neighbourhood of the wall, not necessarily near the separation point. From (10) it follows that

$$\frac{\psi}{U\,\theta} = \tfrac{1}{2}\ell\,\left(\frac{y}{\theta}\right)^2 + \frac{1}{6}\,m\,\left(\frac{y}{\theta}\right)^3 \qquad (11)$$

and hence

$$g = \frac{y_{\psi=0}}{\theta} = \frac{-3\ell}{m}\;;\quad \frac{y_{u=0}}{\theta} = \frac{-2\ell}{m}\;;\quad \frac{y_{u=0}}{y_{\psi=0}} = \frac{2}{3} \qquad (12)$$

An analogous behaviour is shown for solutions with reversed flow of the Falkner-Skan equation

$$F''' + FF'' + \beta\,(1-F'^2) = 0 \qquad (13)$$

This equation describes the similar solutions corresponding to the pressure distribution

$$U = u_1\,x^{m_1} \qquad (14)$$

where u_1 and m_1 are constants.
In (13) F is the non-dimensional streamfunction, primes denote differentiation w.r.t. non-dimensional y; β is the pressure gradient parameter related to m_1 by

$$\beta = \frac{2\,m_1}{m_1+1} \qquad (15)$$

For $\beta>0$ equation (13) only allows solutions with positive skin friction; for $0<\beta<-.198838$ solutions with positive and negative skin friction are possible; $\beta=-0.198838$ represents the separation solution. Extensive tables of solutions with positive skin friction may be found in ref. 19. Some of the reversed flow solutions have been calculated first by Stewartson (ref. 20). Table 1 gives some of the author's own improved results.

Table 1: Some results for reversed flow solutions of Eq. (13)

β	ℓ	m	H	L	$\frac{y_{u=0}}{y_{\psi=0}}$	$g=\frac{y_{\psi=0}}{\theta}$	$-\frac{3\ell}{m}$
-.198838	0	.06815	4.029	.8218	.667	0	0
-.18	-.0545	.05601	5.529	.7343	.667	2.917	2.920
-.10	-.0545	.01503	12.625	.3308	.678	10.665	10.000
-.05	-.0258	.00283	28.096	.1190	.698	25.748	27.350
-.025	-.0106	.00051	59.821	.0418	.721	56.478	62.353

It follows from this table that with a good approximation $\frac{y_{u=0}}{y_{\psi=0}} = 2/3$ and $g = \frac{y_{\psi=0}}{\theta} = -\frac{3\ell}{m}$ as for the velocity profile (10). It should be noted that at the end of the table, corresponding to velocity profiles which are found far downstream in a separation bubble, extremely large values of the shape factor H occur. This is due to the strong increase in δ^* which in turn follows from the thick region with reversed flow. Because the velocities in the separated region remain very small it may be expected that Eq. (8) remains valid within a separation bubble at appreciable distances downstream of separation. This is illustrated by fig. 9 in which a smoke picture of a separation bubble is compared to results of a calculation using Eq. (8). It should be noted that the streamlines can only be calculated when γ is known. In this case the value of γ was taken from the smoke picture.

In ref. 21 it was shown from an extensive empirical investigation that for a wide variety of separated flows it was possible to represent γ by the following simple empirical relation

$$\tan(\gamma) = \frac{B}{\left(\frac{U\theta}{\nu}\right)_{sep}} \qquad (16)$$

where B assumed values between 15 and 20. Later, Wortmann used the relation:

$$B = 64|P| \qquad (17)$$

where P is Gasters pressure gradient parameter for separation bubbles. It should be mentioned here already that our own new series of measurements to be discussed in section 8 is in agreement with (16) for B = 15 to 20 but it does not confirm Wortmann's relation (17). Therefore, in the present paper, we will stick to (16) awaiting clarification of the discrepancy.

Comparing the theoretical result (7) and the empirical result (16) it follows that separating flows

apparently adjust itself such that at separation the following relation is satisfied

$$\tan(\gamma) = \frac{B}{\left(\frac{U\theta}{\nu}\right)_{sep}} = \frac{-3\left(\frac{d\tau_o}{dx}\right)_{sep}}{\left(\frac{\partial p}{\partial x}\right)_{sep}} \qquad (18)$$

Assuming $\frac{\partial p}{\partial y} = 0$ and using Bernoulli's law and the definitions of ℓ and m it follows that

$$\left(\frac{d\ell}{d\bar{x}}\right)_{sep} = \frac{B\frac{d\bar{U}}{d\bar{x}}}{3\bar{U}} = \frac{-B\, m_{sep}}{3(\bar{U}\,\bar{\theta}^2)_{sep}} \qquad (19)$$

We have seen already that slight modifications of the pressure distribution near separation may correspond to rather drastic changes of the boundary layer characteristics. Hence boundary layer calculations, even when based on a measured pressure distribution, may easily fail to reproduce Eq. (19). However, the calculation method described in section 2 may be inverted to find a corrected pressure distribution which does reproduce Eq. (19). For furhter details on this method the reader should be referred to ref. 11.

5. CALCULATION OF THE LAMINAR PART OF THE SEPARATED FLOW.

In reference 21 an approximate method for the calculation of the laminar part of the separated flow was introduced. Essential in this method is that the shape of the separation streamline is prescribed instead of the pressure distribution. The pressure distribution then follows from the calculation. In the earlier version of the method m_{sep} was constant and equal to the Hartree value. In order to maintain compatibility with the present method for attached flows, described in section 2, we should make m_{sep} variabel for the separated flow as well.

To introduce this calculation method for separated flow, reference is made to fig. 10 where ℓ and L have been plotted vs. m for the attached as well as the reversed flow solutions of the Falkner-Skan equation. If it is assumed that the curves in fig. 10 would also apply to a non-similar boundary layer developing from a stagnation point (m=-.08547 , L=0) via the pressure minimum (m=0, L=.44105) and separation (m=.06815 , ℓ=0) downstream into the separated region toward the situation where m=0 , ℓ=0 , L=0, then it follows that $m = -\frac{\theta^2}{\nu}\frac{dU}{dx}$ shows a maximum at separation. Since at separation L is still positive, it follows from the momentum integral equation that θ^2 is still incrasing at separation so that $-\frac{dU}{dx}$ should be decreasing through separation. This leads to an inflexion point in the U vs.x curve slightly upstream of separation. As soon as it is known that there is separation, it is possible to find the separation position by looking for a maximum of m. It can easily be shown from Eqns. (1) and (4) that the condition that m has a maximum at separation leads to:

$$\frac{\bar{U}\frac{d^2\bar{U}}{d\bar{x}^2}}{\left(\frac{d\bar{U}}{d\bar{x}}\right)^2} = \frac{.14026+10\, m_{sep}}{m_{sep}} \qquad (20)$$

Now, the right hand side of Eq. (20) is only slowly varying with m_{sep} and assumes values between 11 and 12 for the values of b and m_{sep} which are of practical interest ($6 < b < 8$; $.075 < m_{sep} < .15$). Hence the separation position can be found from $\bar{U}(\bar{x})$ by looking for the value of $\bar{x}$ where the left hand side of Eq. (20) assumes values between 11 and 12. For a number of experiments this gave a very good indication of the separation point. A calculation method for the reversed flow region, which is comparable to that for attached flow described in section 2, could now be developed if also for reversed flows the characteristic parameters L, ℓ and H would be given functions of m/m_{sep}. Since, except for the Stewartson profiles, no exact results for separated flows were available to the author these functions have been "guessed" as follows. For ℓ it was assumed that ℓ is a universal function of m/m_{sep} given by the Stewartson profiles, where m_{sep} follows from the calculation up to the separation point. For L(m) a curve was assumed which is very similar to that for the Stewartson flows namely: tangent to L=a+bm at separation, tangent to the vertical axis at m=0, L=0 (fig. 10) and super-elliptic in between. This leads to:

$$\left(\frac{m_{sep}-m}{m_{sep}}\right)^n + \left(\frac{L-bm}{a}\right)^n = 1 \quad \text{or} \quad L = bm + a\left\{1-\left(1-\frac{m}{m_{sep}}\right)^n\right\}^{\frac{1}{n}} \qquad (21)$$

where the exponent n was taken equal to the value 1.65 which was found to give a good representation of the Stewartson results. If necessary H can be found from m, ℓ, L and the definition of L.

Since in the separated region the shape of the separation streamline will be prescribed it appears that the proper velocity profile shape parameter is $g = \frac{y_{\psi=0}}{\theta}$. Using the approximation $g = -3\ell/m$ (Eq. 12) and observing that ℓ is assumed to be a universal function of m/m_{sep} it follows that we should use $z = g * m_{sep}$ where m/m_{sep} is a universal function of z.

The shape of the separation streamline can be prescribed in a number of different ways. In many applications we used a straight separation streamline, leaving the wall at an angle γ given by Eq. (16) with B = 15 to 20. Since in most cases the separation streamline is slightly curved upwards in the laminar region (see for instance fig. 9) a better approximation may be obtained by assuming a linear variation of g with x downstream of separation. Since θ is still increasing in the bubble it follows that this leads, together with the linear variation of g, to a separation streamline which is slightly curved upwards. In general the results do not differ much for both cases. It should be remarked that any shape of the separation streamline could be prescribed without difficulty. Summarising, the separated flow can be calculated as follows once m_{sep} and proper starting values for θ and U are given (for instance at separation).

1. Find g from θ and the prescribed shape of the separation streamline.
2. Find m/m_{sep} from the universal relation between $z=g*m_{sep}$ and m/m_{sep}.
3. Find $\frac{dU}{dx}$ from the first compatibility condition in the form $\frac{dU}{dx} = -m\nu/\theta^2$.
4. Find $\frac{d}{dx}(\frac{\theta^2}{\nu})$ from the momentum integral relation.
5. Advance a step in x-direction and find new starting values for U and θ, etc.

Full details of the method will be presented in ref. 11; some examples will be given in section 8.

6. PREDICTION OF THE LOCATION OF TRANSITION IN THE SEPARATED FLOW.

For attached flows the position of transition can be predicted by means of a semi-empirical method which is based on the calculation of the amplification of small disturbances in the laminar boundary layer. This method was developed independently by Smith and Gamberoni (ref. 22) and the present author (ref. 23 and 24). In ref. 24 it was shown that the method is also applicable to boundary layers with suction. The idea behind the method is that the calculated amplification ratio of the most critical disturbance at the measured transition position attains nearly always the same value.

At present we are investigating whether this method is also valid for separated flows. This investigation is based on the stability diagrams for some of the Stewartson velocity profiles with reversed flow which have been published recently by Taghavi and Wazzan (ref. 25).

Since these calculations have been restricted to rather low values of R_θ the results have been supplemented by calculating the limiting stability characteristics for $R_\theta \to \infty$ using the inviscid stability equation (Rayleigh equation). These calculations have been performed on one of the hybrid computers of the Delft University Computing Centre.

Both Wazzan's and our own computations were made for the linear stability theory in the spatial mode. This means that in the expression for the streamfunction of the disturbance

$$\psi(x,y,t) = \varphi(y)\, e^{i(\alpha x-\omega t)} \qquad (22)$$

α is complex $= \alpha_r + i\,\alpha_i$ and ω is real. This leads to a factor $e^{-\alpha_i x}$ in the amplitude of the disturbance. Hence the logarithm of the total amplification of a disturbance follows from:

$$\sigma_a = \ell n \frac{a}{a_{neutral}} = \int -\alpha_i \, dx \qquad (23)$$

Application of the semi-empirical method for the prediction of transition requires the evaluation of Eq. (23) for a range of reduced frequencies $\frac{\omega\nu}{U^2}$ to select the most dangerous frequencies. The available time for the preparation of the present paper did not permit to perform these detailed amplification calculations for the experimentally determined pressure distributions. However, we developed a short-cut method which is thought to provide a reasonably accurate first estimate of the transition position in the separated flow at rather low values of the Reynoldsnumber, where no appreciable amplification occurs prior to separation. This short-cut method will be described in the remainder of the present section. Some examples will be discussed in section 8.

It may be assumed with reasonable accuracy that in the laminar part of the separation bubble θ, U and R_θ are constant and equal to their values at separation. Then constant values of

$$\frac{\omega\nu}{U^2} = \frac{\frac{\omega\theta}{U}}{\frac{U\theta}{\nu}}$$

also mean constant values of $\frac{\omega\theta}{U}$.

Furthermore it may be assumed that downstream of separation g is proportional to $x-x_{sep}$ with:

$$g = \frac{y_{\psi=0}}{\theta} = \frac{(x-x_{sep})\tan(\gamma)}{\theta} = \frac{(x-x_{sep})}{\theta}\frac{B}{(R_\theta)_{sep}} \tag{24}$$

Hence Eq. (23) may be written as:

$$\sigma_a = \frac{(R_\theta)_{sep}}{B\, m_{sep}} \int (-\alpha_i\theta)\, d(g \times m_{sep}) = \frac{(R_\theta)_{sep}}{B\, m_{sep}} \int (-\alpha_i\theta)dz \tag{25}$$

so that the integration with respect to x has been replaced by an integration w.r.t. g. Similarly we can over a short interval upstream of separation, assuming ℓ to be proportional to $x_{sep}-x$, perform the integration w.r.t. ℓ instead of x. Now we make the further assumption that the Reynoldsnumber is so high that the stability characteristics are given with sufficient accuracy by the limiting values determined from the inviscid stability equation. Then $-\alpha_i\theta$ only depends on the value of $\frac{\omega\theta}{U}$ and the profile parameter β or z. Hence the integration w.r.t. z in Eq. (25) can be performed once for all independently of $(R_\theta)_{sep}$ or the pressure distribution for different values of $\frac{\omega\theta}{U}$. A similar result holds for the integration w.r.t. ℓ upstream of separation.

The inviscid instability for different values of β is shown in figs. 11a and 11b. Values of $10^4\int(-\alpha_i\theta)dz$ are shown in fig. 12 for different values of $\frac{\omega\theta}{U}$ together with the envelope giving the maximum value I of the integral as a function of z. Hence the maximum amplification factor σ_a follows from (25) in the form

$$\sigma_a = 10^{-4}\frac{(R_\theta)_{sep} I}{B.m_{sep}} \tag{26}$$

According to previous experience with the transition prediction method it may be expected that transition will occur in practice as soon as the calculated value of σ_a exceeds a critical value which is of the order of 10.

A further simplification results when I(z) is replaced by the approximation (see fig. 13)

$$I = 650\sqrt{z} \tag{27}$$

Eq. (27) completely neglects the amplification upstream of separation but is rather accurate for large values of z. Combining Eqs. (26), (27) and (24) it follows that the position of transition x_{tr} follows from

$$\frac{x_{tr}-x_{sep}}{\theta_{sep}} = \frac{\sigma_a^2\, 10^8\, B\, m_{sep}}{650^2\,(R_\theta)_{sep}} = \frac{237\,\sigma_a^2\, B\, m_{sep}}{(R_\theta)_{sep}} \tag{28}$$

Using as mean values B=17.5; m_{sep}=0.10 and σ_a=14.4 (see section 8) we find:

$$\frac{x_{tr}-x_{sep}}{\theta_{sep}} = \frac{8.6\times10^4}{(R_\theta)_{sep}} \tag{29}$$

7. POSSIBLE METHODS TO PREDICT BURSTING OF THE BUBBLE.

A number of methods may be used to predict whether reattachment of the shear layer will occur downstream of transition. A few of these methods will be briefly described in this section; some experimental checks will be given in section 8.

In ref. 6 Crabtree observed that there seems to be a maximum limit to the pressure rise which a reattaching turbulent shear layer may overcome. From a number of experiments he deduced that the pressure coefficient

$$\sigma = 1 - \left(\frac{Ur}{u_{sep}}\right)^2 \tag{30}$$

is nearly constant for short bubbles about to burst; the constant value he suggested was 0.35. Since it seems better to correlate different experimental results on the pressure rise between transition and reattachment we will use a slightly different coefficient σ_{cr} defined by:

$$\sigma_{cr} = 1 - \left(\frac{Ur}{U_{tr}}\right)^2 \tag{31}$$

If Eq. (30) or (31) is to be used to predict whether reattachment will occur, the value of U_r at the possible reattachment point has to be known. In a first approximation this may be taken from the pressure distribution which would occur without the bubble being present at the position x_{tr}, (the "inviscid pressure distribution").

In ref. 26 Horton gave a method to predict whether and where reattachment may occur. This method is based on the simple criterion that $(\frac{\theta}{U}\frac{dU}{dx})_r$ = constant = -.0082 for all reattaching turbulent shear layers.

A simple criterion for bursting is provided by Stratford's zero skin friction limiting pressure distribution, (ref. 27). This is the adverse pressure distribution which a turbulent boundary layer can just negotiate without separation. This limiting pressure distribution curve, starting at the measured transition point T (fig. 1) can at low Reynoldsnumber fail to cross the "inviscid pressure distribution curve". This means that the requested pressure rise is more than the Stratford pressure recovery can provide, and hence bursting occurs. For our experimental results on the Wortmann airfoil (section 8) this gave a very good prediction of the bursting Reynoldsnumber.

8. SOME EXPERIMENTAL RESULTS.

Two series of experiments were performed. The first one was on the FX 66-S-196-V1 Wortmann airfoil at an angle of attack of 1 degree in a small 400 x 400 mm windtunnel. The chordlength of the airfoil was 360 mm. The second investigation concerned a 400 mm dia. circular cylinder with a tail (to suppress a fluctuating wake) in the large 1810 x 1250 mm low turbulence windtunnel (model configuration c, ref. 21).

Fig. 14 shows some of the pressure distributions for the airfoil at different Reynoldsnumbers; bursting occurs between R_c=.118 and .099 $\times 10^6$. An extensive series of flow pictures, similar to that shown in fig. 9, was made using the special camera described in ref. 21. Fig. 15 shows a plot of tan(γ) vs.$(R_\theta)_{sep}$; the region of $(R_\theta)_{sep}$ at which bursting occurs is indicated in the figure. It follows that before and after bursting B lies always between 15 and 20.
Gaster's pressure gradient parameter P is shown in the lower half of fig. 16 for the closed bubbles. Extrapolation of this curve to the first value of $(R_\theta)_{sep}$ measured after bursting would give a point beyond Gasters bursting line. It follows that $-.185 < P < -.120$ so that Wortmann's relation (Eq. 17) would give $7.7 < B < 11.8$ which is not in agreement with fig. 15.
The upper half of fig. 16 shows the pressure recovery coefficient between transition and reattachment. It follows that the maximum value of σ_{cr}=0.36 which is obtained just prior to bursting is in good agreement with Crabtree's suggested maximum of 0.35.
Figs. 17 and 18 show the pressure distributions in the region of the bubble for the highest and lowest Reynoldsnumber at which a closed bubble was observed. The curve labelled B=15 is the result of a calculation using the method discussed in section 5 with a straight separation streamline. Results for a linear variation of g and/or B=20 are only slightly different. It is seen that the best fit is obtained at the highest Reynoldsnumber; results for 6 intermediate values of R_c show a gradual change from the results shown in fig. 17 to those of fig. 18. The curves labelled "Horton" indicate the locus of possible reattachment points. Where this curve crosses the "inviscid pressure distribution" indicated by a dotted curve, a closed bubble is obtained. It follows that Hortons method indicated bursting already in fig. 18. Results for the intermediate Reynoldsnumbers show that bursting is indicated too early by this method. It is possible that a modification of the constants in Horton's method would lead to a better result; this has not been attempted however. The curves labelled Stratford indicate Stratfords limiting pressure distribution starting from the measured transition point. It follows from fig. 18 that according to this method the bubble is about to burst at R_c=.118 $\times 10^6$; this is in agreement with experimental observation.
The length of the laminar part of the bubble is shown in fig. 19 as a function of R_c. The broken curve indicates the predicted length for σ_a=12.5 and B=15 using the method of section 6 where I(z) is taken from fig. 12.

Results similar to those for the Wortmann airfoil have been obtained for the cylindrical model. In this case only short bubbles have been measured on the cylindrical part. Fig. 20 shows the length of the laminar part of the bubble; included in the figure are calculated curves for B=15 and 20, using the value σ_a=12.5 which was found to correlate well the measurements for the airfoil at B=15. It follows that in general the bubble is longer on the cylinder than on the airfoil. From some further calculations, the results of which are not shown in the figures, it follows that for a mean value B=17.5 the value of σ_a is about 11.7 for the airfoil and 14.4 for the cylinder.
Figure 21 shows a comparison of both series of results in the form of $\frac{\Delta x}{\theta}$ vs.$(R_\theta)_{sep}$ where Δx is the length of the laminar part of the bubble and $\theta = \theta_{sep}$. Besides the measured points some calculated curves are shown together with an empirical correlation curve which was given by Vincent de Paul in ref. 28. It follows that

the different measurements do not correlate very well so that some other parameter should be of importance. An important difference between our own two series of measurements is that they have been obtained in two different windtunnels. The airfoil was tested in a small tunnel where the noise level, the amount of vibration and possibly the free stream turbulence intensity are much higher than in the large low turbulence tunnel. The large tunnel was very quiet at the low speeds used, while at these low speeds the turbulence level is of the order of .02%. To check whether the noise in the small tunnel could have caused earlier transition, the noise at different speeds was recorded on a tape recorder and reproduced in front of an open window in the test section of the large tunnel. This had a marked effect on transition; the length of the separated region decreased by about 1 degree at high speeds and by about 3 degrees at the lowest speed. The corresponding decrease in $\frac{\Delta x}{\theta}$ ranged from 35 to 50; the value of σ_a which correlates the measurements at B=17.5 decreased from 14.4 for the quiet situation to 13.1 with the noise. (see also fig. 21)
In a further experiment the cylindrical model was subjected to tones recorded from an electronic organ; it proved possible to obtain the same reductions of the distance to transition if only at each speed the proper frequency was used. These frequencies correlated rather well with the dangerous frequencies which can be obtained from fig. 12. Of course there may be other variables like longitudinal surface curvature, mechanical vibrations, free stream turbulence level, etc. which have to be taken into account.
For the time being it is suggested that transition in the bubble can be calculated for "quiet" flows using the method of section 6 with mean values B=17.5; σ_a=14.4; m_{sep}=0.10.

9. REFERENCES.

1. Tani, I.: Low speed flows involving bubble separation. Progr. in Aeron. Sc., Vol 5, p 70-103, Pergamon Press, 1964.
2. Chang, P.K.: Separation of Flow, Pergamon Press, 1970.
3. Young, A.D. and Horton, H.P.: Some results of investigations of separation bubbles. In: AGARD CP4 Separated Flows, 1966, part 2, p 779-811.
4. Gaster, M.: The structure and behaviour of laminar separation bubbles. In:AGARD CP4, Separated Flows, 1966, part 2, p 813-854.
5. Brown, S.N. and Stewartson, K.: Laminar separation. In: Annual Review of Fluid Mechanics, vol 1, Palo Alto, Annual Reviews Inc., 1969, p 45-72.
6. Crabtree, L.F.: The formation of regions of separated flow on wing surfaces. R and M 3122, 1959.
7. Thwaites, B.: Approximate calculation of the laminar boundary layer. Aeron. Quart, 1, p 245-280, 1949.
8. Head, M.R.: An approximate method of calculating the laminar boundary layer in two-dimensional Incompressible flow. R and M 3123, 1959.
9. Stratford, B.S.: Flow in the laminar boundary layer near separation. R and M 3002, 1957.
10. Curle, N. and Skan, S.W.: Approximate methods for predicting separation properties of laminar boundary layers. Aeron. Quart, 8, p 257-268, 1957. See also: Curle, N.: The estimation of laminar skin friction, including the effects of distributed suction. Aeron. Quart, 11, p 1-21, 1960.
11. Ingen, J.L. van: ... (a report on the method for calculating the separating laminar boundary layer, discussed in the present paper). To be published in the series of VTH-reports of the Dept. of Aeron.-Eng., Delft University of Technology.
12. Terrill, R.M.: Laminar boundary layer flow near separation with and without suction. Phil.Trans. A 253, 1960, p 55-100.
13. Goldstein, S.: On laminar boundary layer flow near a position of separation. Quart. J. Mech. Appl. Math. Vol 1, 1948, p 43-69.
14. Hartree, D.R.: The solution of the equations of the laminar boundary layer for Schubauer's observed pressure distribution for an elliptic cylinder. R and M 2427, 1939.
15. Carter, J.E.: Solutions for laminar boundary layers with separation and reattachment. AIAA paper 74-583, 1974.
16. Legendre, R.: Décollement laminaire régulier. Comptes Rendus 241, 1955, p 732-734.
17. Oswatitsch, K.: Die Ablösungsbedingung von Grenzschichten. In: Grenzschichtforschung/Boundary layer research. IUTAM Symposium, Freiburg / Br. 1957, Springer Verlag 1958, p. 357-367.
18. Batchelor, G.K.: An introduction to fluid dynamics, Cambridge Univ. Press, 1970.
19. Smith, A.M.O.: Improved solutions of the Falkner-Skan boundary layer equation. Sherman M. Fairchild Fund Paper FF-10, Inst. Aero. Sci. 1954.
20. Stewartson, K.: Further solutions of the Falkner-Skan equation. Proc. Cambr. Phil.Soc, 50, p 454-465, 1954.
21. Dobbinga, E., Ingen, J.L. van, Kooi, J.W.: Some research on two-dimensional laminar separation bubbles. AGARD CP-102, paper nr. 2, Lisbon 1972.
22. Smith, A.M.O. and Gamberoni, N.: Transition, pressure gradient and stability theory. Report ES 26388, Douglas Aircraft Co., 1956.
23. Ingen, J.L. van: A suggested semi-empirical method for the calculation of the boundary layer transition region. Report VTH-74, Dept. of Aeron. Eng., University of Technology Delft, 1956.
24. Ingen, J.L. van: Theoretical and experimental investigations of incompressible laminar boundary layers with and without suction. Report VTH-124, Dept. of Aeron. Eng., University of Technology Delft, 1965.
25. Taghavi, H. and Wazzan, A.R.: Spatial stability of some Falkner-Skan profiles with reversed flow. Physics of Fluids, Vol 17, no 12, Dec. 1974, p 2181-2183.
26. Horton, H.P.: A semi-empirical theory for the growth of laminar separation bubbles. A.R.C.-CP 1073, 1967.
27. Stratford, B.S.: The prediction of separation of the turbulent boundary layer. Journal of Fluid Mechanics, Vol 5, pt 1, january 1959, p 1-16.
28. Vincent de Paul, M.: Prevision du decrochage d'un profil d'aile en écoulement incompressible. Paper nr. 5 in AGARD, CP-102, Lisbon, 1972.
29. Wortmann, F.X.: Ueber den Ablösewinkel laminarer Ablöseblasen. DLR-FB-74-62, 1974.
30. Wortmann, F.X.: The quest for high lift. AIAA paper 74-1018, 1974.

ACKNOWLEDGEMENT.

The author is indebted to many persons who in one way or another assisted in the investigations reported in this paper.

The technical staff of the Department of Aeronautical Engineering gave their able assistance during the preparation and execution of the experimental stages of the work. Especially Mr. P. Smit should be thanked for his continuous technical support.

Ir. J.J.H. Blom gave his expertness in obtaining and interpreting surface oil film patterns to determine positions of separation and reattachment. Ir. E. Dobbinga should be thanked for his perseverance to obtain smoke pictures of the highest quality.

Mr. R. Llurba of the Delft University Computing Centre performed the hybrid computations leading to figs. 11a and 11b.

Finally prof. A.R. Wazzan should be thanked for sending an advance copy of ref. 25 and some tabular material related to his paper.

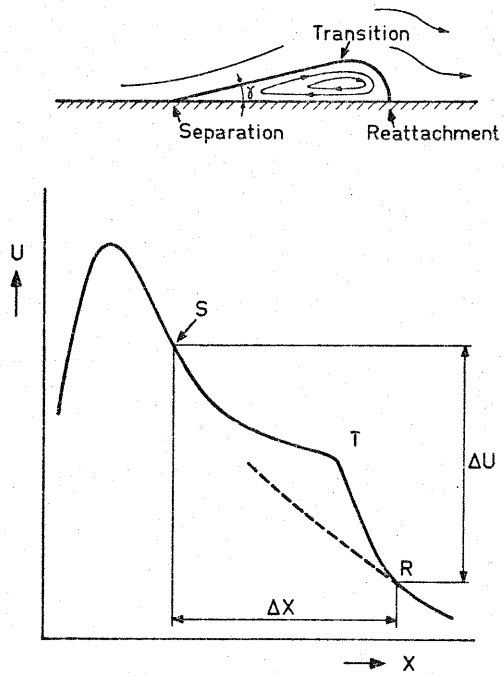

Fig. 1: Schematic diagram of flow field and pressure distribution in a laminar separation bubble.

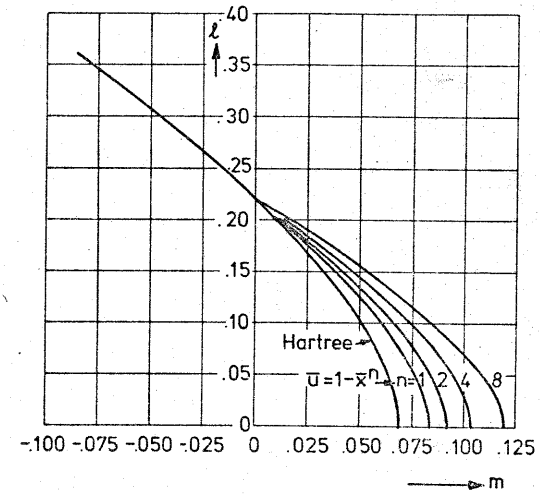

Fig. 2: ℓ(m) for some special exact solutions of the boundary layer equations.

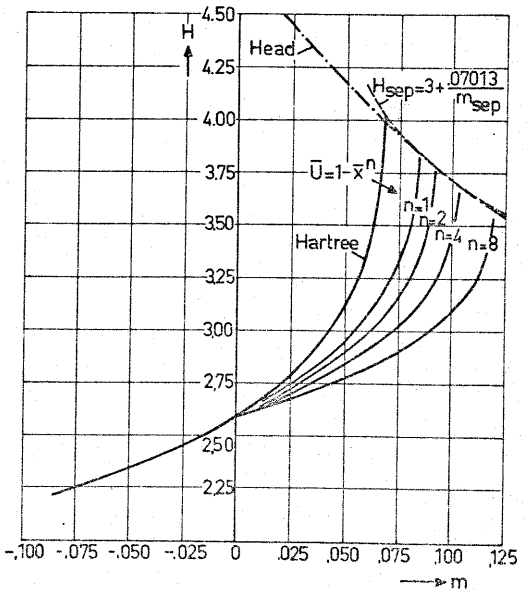

Fig. 3: H(m) for some special exact solutions of the boundary layer equations.

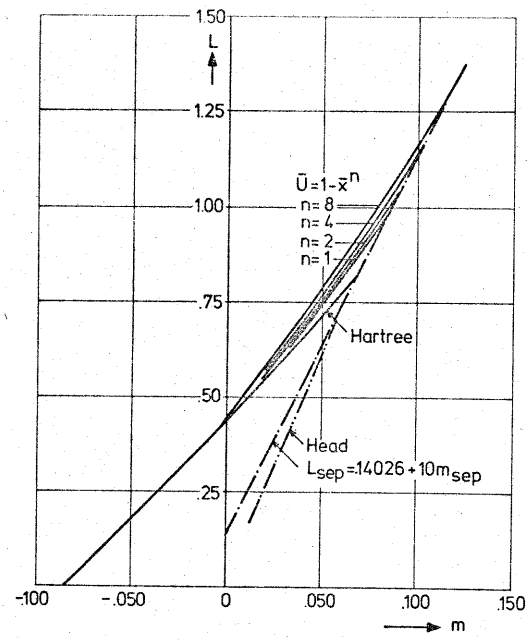

Fig. 4: L(m) for some special exact solutions of the boundary layer equations.

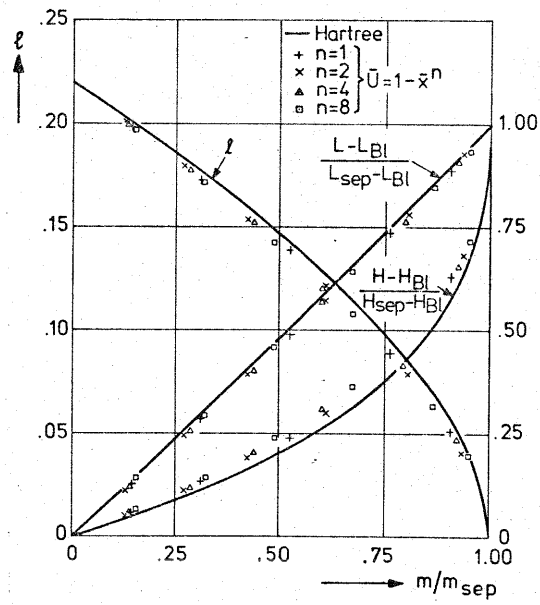

Fig. 5: ℓ(m), H(m) and L(m) in normalised form for some special exact solutions of the boundary layer equations (m>0).

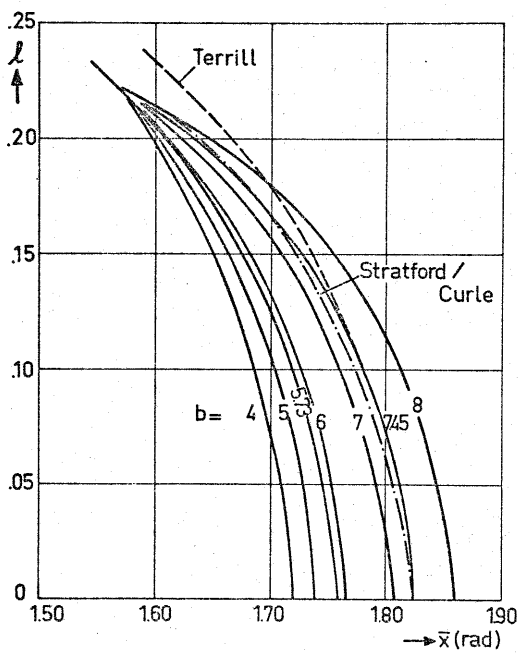

Fig. 6: Some results of the present method for the potential flow pressure distribution for a circular cylinder $\bar{U}=\sin(\bar{x})$ compared to the results according to Terrill (ref. 12) and Curle/Skan (ref. 10).

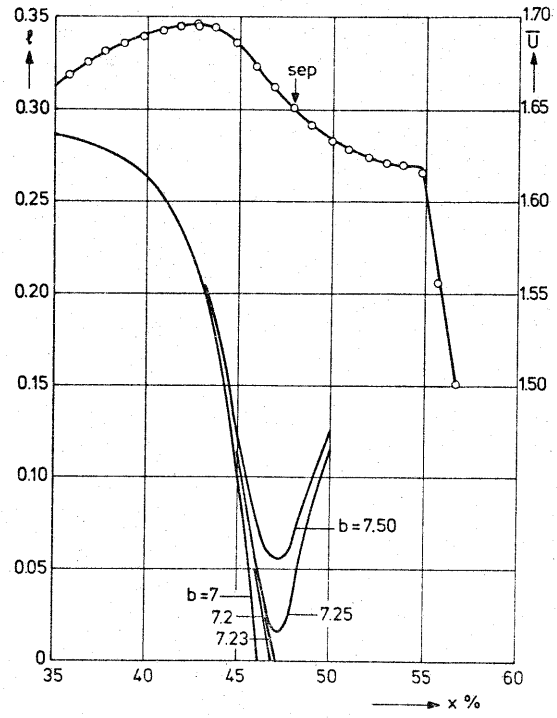

Fig. 7: $\bar{U}$ (uppercurve) and ℓ (lower curves) for the Wortmann airfoil; $R_c=.638 \times 10^6$, $\alpha=1^o$.

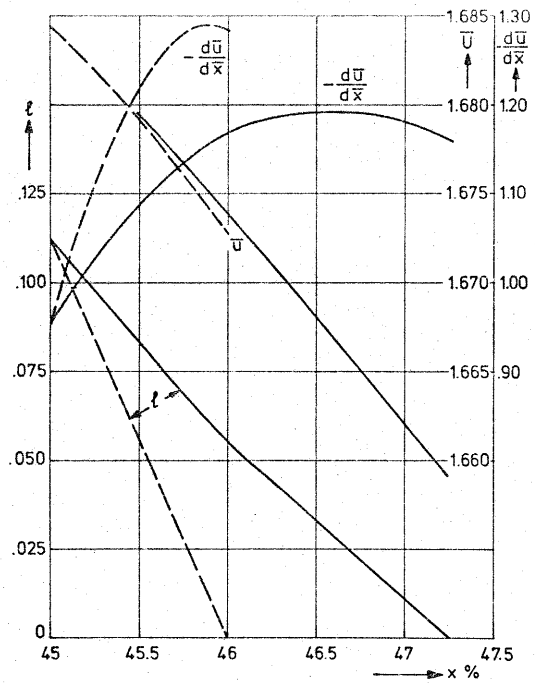

Fig. 8: Modification of the pressure distribution which is required to produce a given change in $\ell(x)$. Wortmann airfoil: b=7.23; R_c=.638 × 10^6; α=1°; for x<45% same $\bar{U}$ and ℓ as in fig. 7.

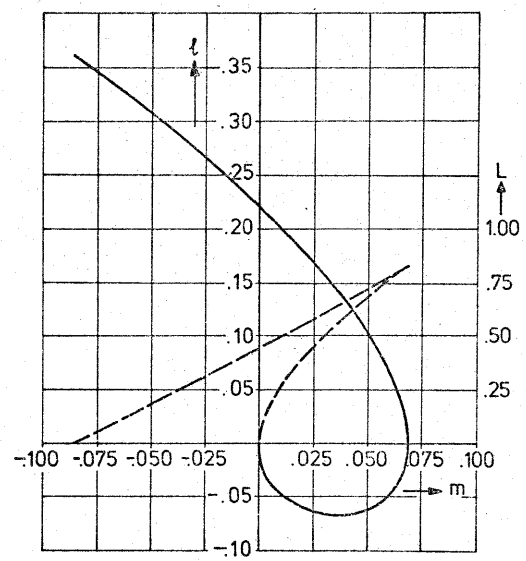

Fig. 10: ℓ(m) ——— and L(m)----- for Hartree's and Stewartson's solutions of the Falkner-Skan equation.

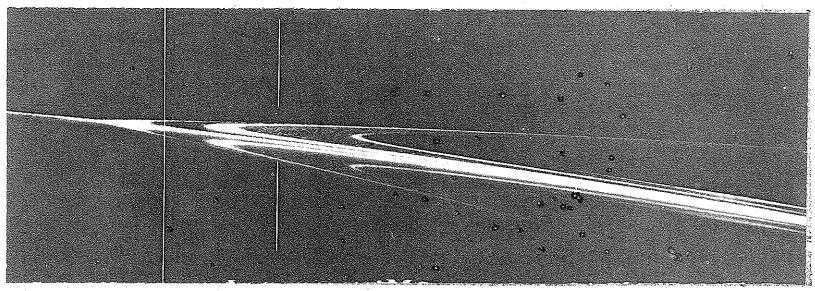

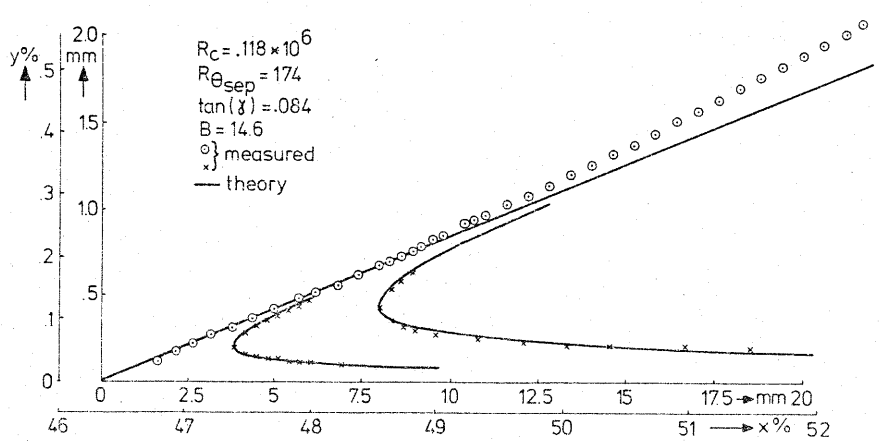

Fig. 9: One of the smoke pictures obtained for the Wortmann airfoil and comparison with Eq. (8).

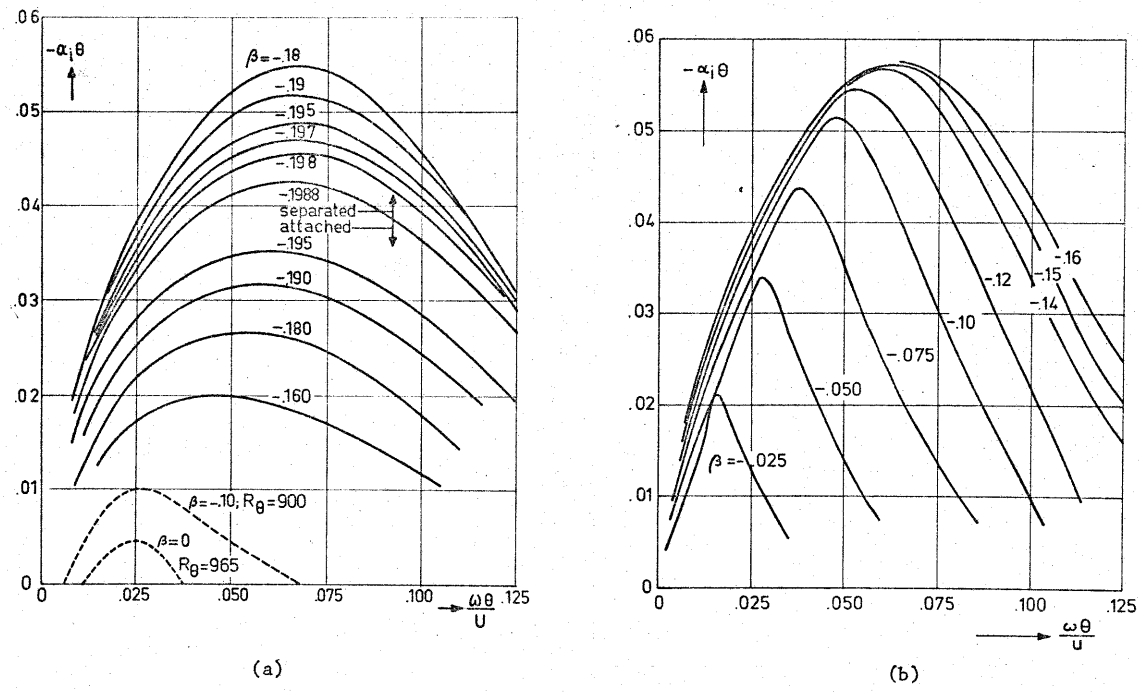

Fig. 11 a and b: Inviscid instability for Hartree's and Stewartson's velocity profiles. For $\beta=0$ and $-.10$ the inviscid instability becomes very small. For comparison the viscid instability is shown for R_θ of the order of 1000.

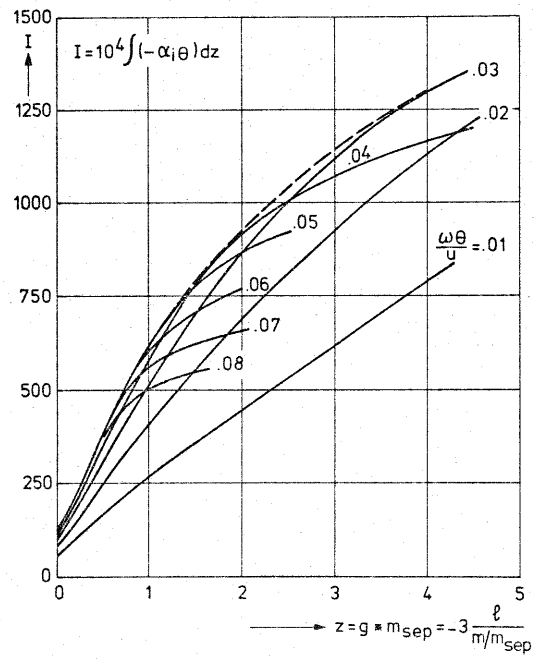

Fig. 12: Normalised amplification integral; see Eq. (25).

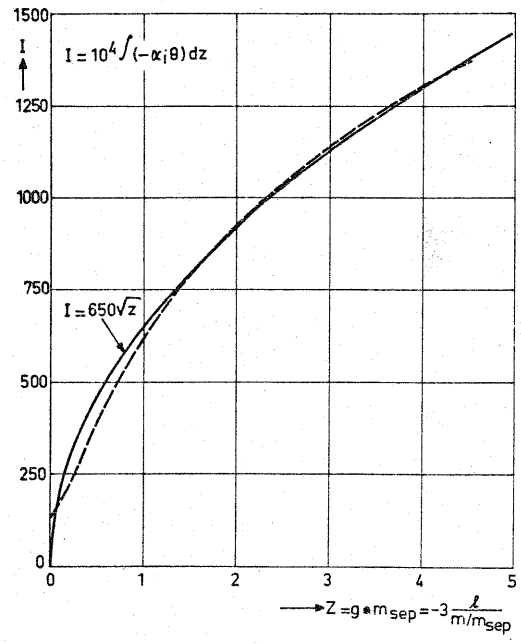

Fig. 13: Approximation to the amplification integral.

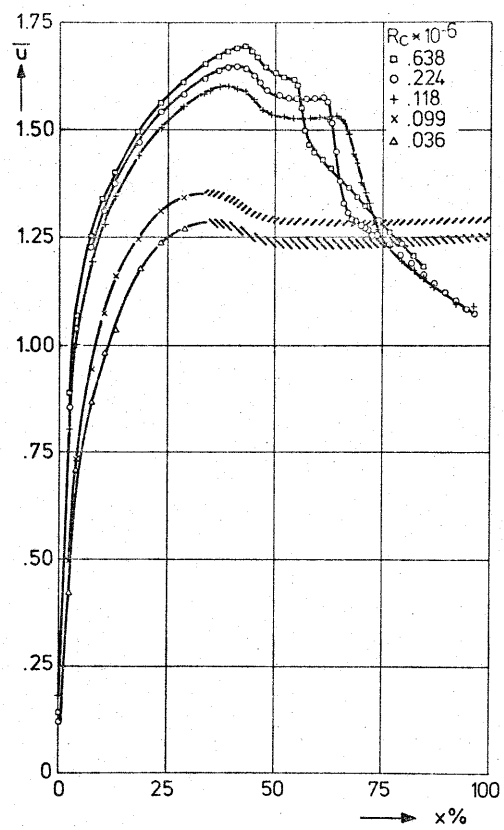

Fig. 14: Some of the measured pressure distributions for the Wortmann airfoil (for $R_c \leq .099 \times 10^6$ the bubble bursts).

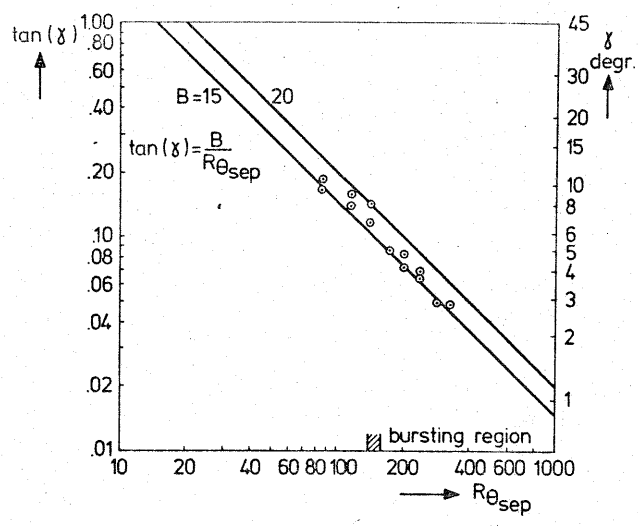

Fig. 15: $\tan(\gamma)$ vs. $R\theta_{sep}$ for the Wortmann airfoil.

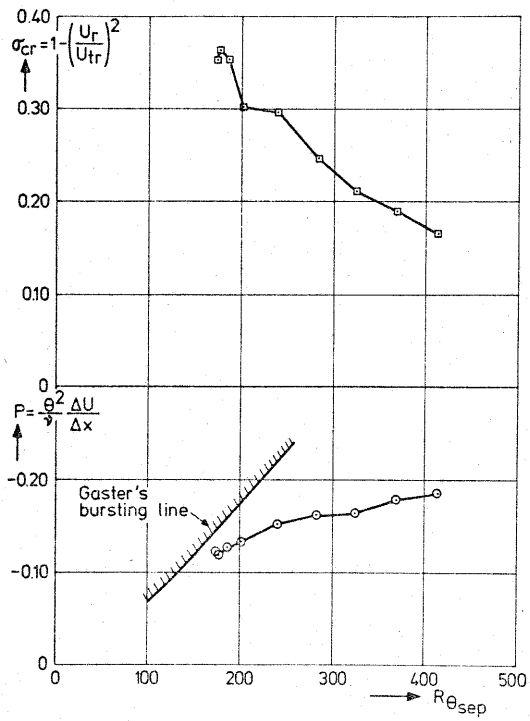

Fig. 16: Pressure recovery coefficient σ_{cr} (Eq. 31) and Gasters pressure gradient parameter for closed separation bubbles on the Wortmann airfoil.

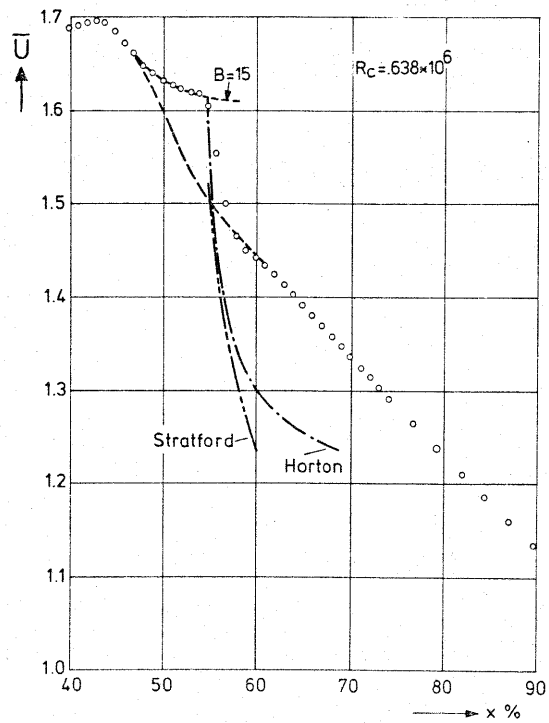

Fig. 17: Some results for the Wortmann airfoil at $R_c=.638 \times 10^6$.

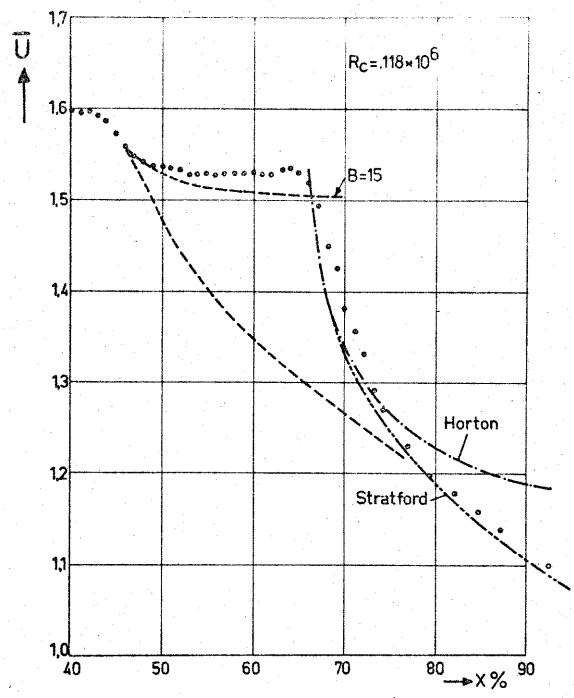

Fig. 18: Some results for the Wortmann airfoil at R_c=.118 × 10^6.

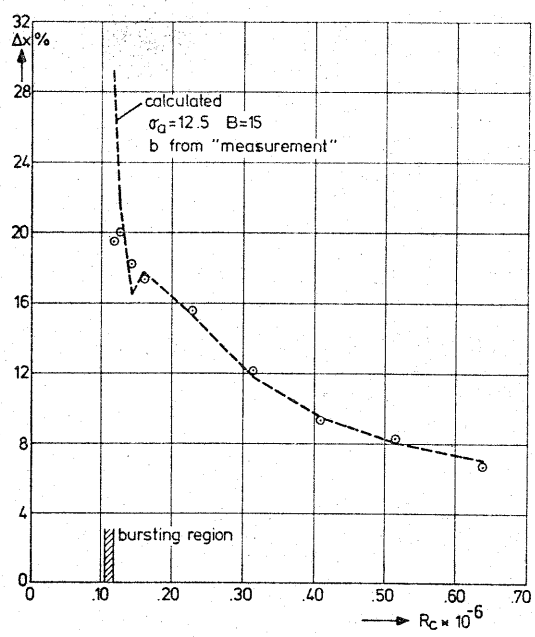

Fig. 19: Length of the laminar part of the separation bubble on the Wortmann airfoil.

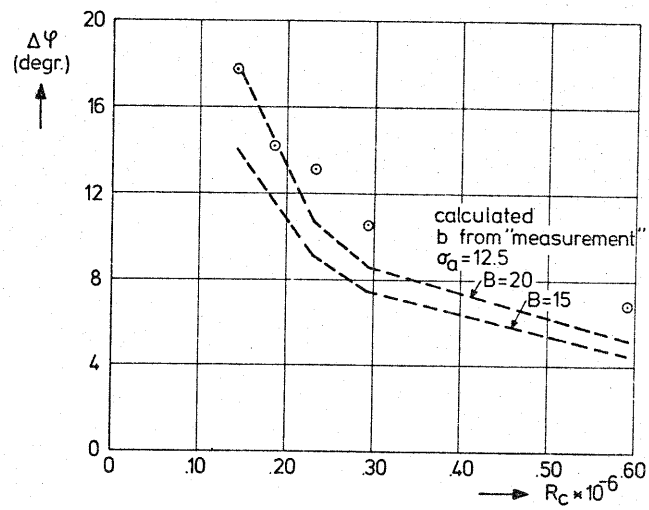

Fig. 20: Length of the laminar part of the separation bubble on the circular cylinder with tail.

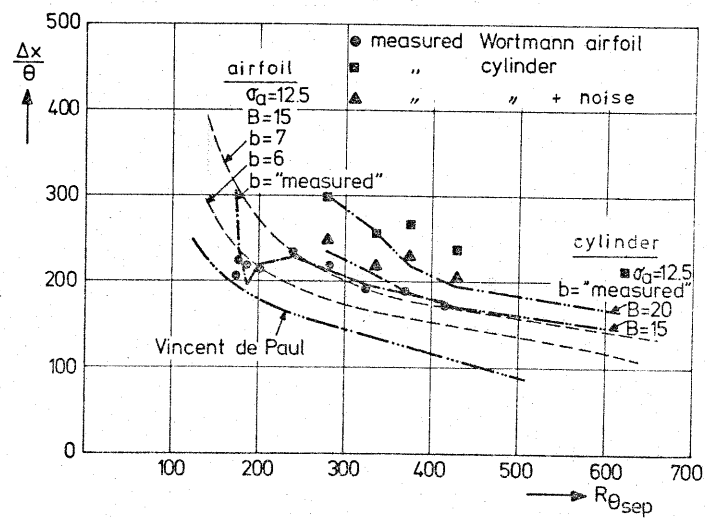

Fig. 21: $\Delta x/\theta_{sep}$ as function of $(R_\theta)_{sep}$ Measured points for the Wortmann airfoil (●) and the cylinder with (▲) and without (■) extra noise. Curve labelled "Vincent de Paul" denotes the correlation curve used in ref. (28).